Preliminary Computational Assessment of Disk Rotating Detonation Engine Configurations

Daniel E. Paxson*
NASA Glenn Research Center, Cleveland, Ohio, 44130

A rotating detonation engine (RDE) configuration whereby the working fluid enters and exits in a predominantly radial manner is examined using a quasi-two-dimensional computational fluid dynamic simulation. The simulation, based on a Cartesian coordinate system, was originally developed to examine the physics and performance of the more typical annular RDE. Modifications required to accommodate the radial and circumferential flowfield are discussed. The centripetal forces that arise in this disk RDE (DRDE) configuration create a different wave structure than that seen in the annular RDE. They also give rise to markedly different fluid behavior depending on whether the flow is radially inward or radially outward. Using an entropy-based measure of pressure gain, it is found that for the preliminary idealized calculations performed in this paper, the inward flowing DRDE outperforms the outward flowing variant. The inward flowing DRDE is further shown to outperform the equivalent annular RDE. The effects on performance of several parameters are examined, including inner-to-outer diameter ratio, inner-to-outer cross-sectional area ratio, and inlet throat-to-channel area ratio.

Nomenclature

A_{ch}	=	channel cross-sectional area near the inlet
A_i	=	inlet restriction cross-sectional area
a	=	non-dimensional speed of sound
a^*	=	reference speed of sound
D_i	=	inner diameter
D_o	=	outer diameter
EAP_i	=	Equivalent Available Pressure (ideal)
EEP	=	Entropy Equivalent Pressure
h	=	channel height
h_o	=	channel height at the outer diameter
h_f	=	fuel heating value
K_0	=	reaction rate constant
l	=	circumference
p	=	non-dimensional pressure
p^*	=	reference pressure
PG	=	pressure gain
R_g	=	real gas constant
s	=	non-dimensional entropy
T	=	non-dimensional temperature
T^*	=	reference temperature
t	=	non-dimensional time
t_{cycle}	=	non-dimensional time for one detonation wave revolution
t_{output}	=	non-dimensional time interval associated with computational output
u	=	non-dimensional x-component velocity
U^n	=	non-dimensional velocity component normal to a grid face
u_{det}	=	non-dimensional detonation velocity

*Aerospace Research Engineer, Research and Engineering Directorate, 21000 Brookpark Road, AIAA Associate Fellow

v = non-dimensional y-component velocity
x = non-dimensional horizontal dimension
y = non-dimensional vertical dimension
z = reactant fraction

Greek
γ = ratio of specific heats
φ = generic quantity
ρ = non-dimensional density
ρ^* = reference density

Subscripts
exit = exit flow boundary
i = x-grid index
j = y-grid index
k = output time interval index
m = manifold (inlet)
t = total

Overbar
$\bar{\ }$ = denoting mass flux-averaged

I. Introduction

Research is currently underway in the pressure gain combustion (PGC) community investigating rotating detonation engine (RDE) configurations where the fluid flow is predominantly radial, and the detonation propagation is circumferential. The basic arrangements for these disk RDE's (DRDE's) are illustrated in Fig. 1. Bulk flow is either radially inward or radially outward. For the radially inward configuration (Fig. 1, left), fuel and oxidizer enter the channel at the outer diameter, and are processed by a circumferentially propagating detonation also anchored at the outer diameter. Exhaust products exit the channel predominantly radially at the inner diameter, and are subsequently turned in the axial direction by a turbine or nozzle (not shown) before exiting the device. For the radially outward configuration (Fig. 1, right), fuel and oxidizer enter the device axially and are turned in the radial dirction by a presumed diffuser or impeller (not shown) to enter the channel at the inner diameter. They are subsequently processed by a circumferentially propagating detonation anchored at the inner diameter. Exhaust products exit the channel and device predominantly radially at the outer diameter. The cross-sectional flow area (i.e. normal to the radial direction) may vary with radius. The outer-to-inner diameter ratio may also vary. The DRDE configuration has potential benefit with compact radial turbomachinery PGC applications [1-3] or propulsion applications where

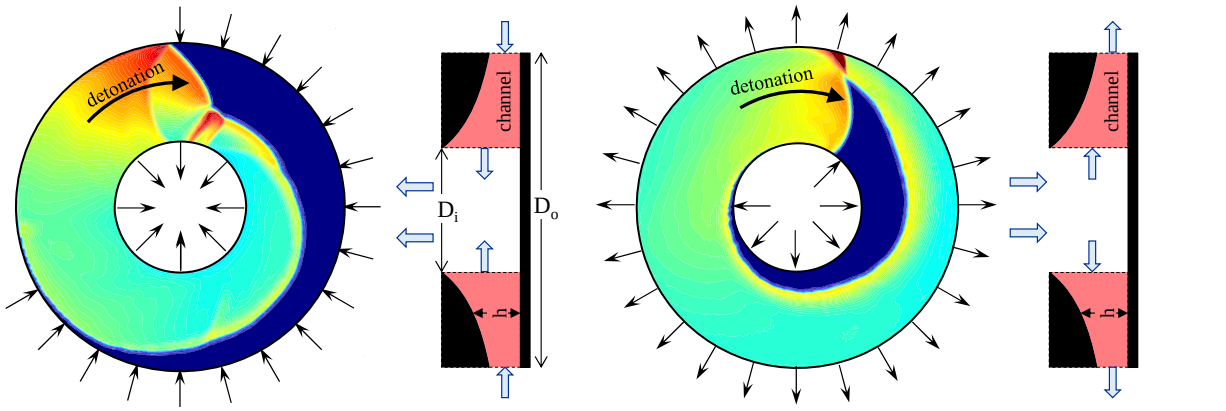

Fig. 1 Basic configurations for disk rotating detonation engines (DRDE). The flow fields are illustrated using contours of temperature. The channel height dimension is enlarged for visibility relative to the diameter.

length is constrained. There is additionally some evidence that the centripetal forces arising in DRDE configurations enhance stable operation [4].

Most of the DRDE research to date is experimental, and focused primarily on achieving repeatable detonation cycles. The question of performance (i.e. measurable pressure gain) from the device itself is not addressed. It is the goal of this paper to take a preliminary step in this direction using computational fluid dynamic (CFD) simulations. The CFD environment is advantageous for assessing performance potential since it allows secondary losses to be eliminated from consideration, provides flowfield information that cannot be measured in experiments, and can facilitate rapid parametric variation for assessing the impact of configuration changes on performance. In essence, it helps ascertain whether the DRDE concept is advantageous in principle as opposed to whether a particular experiment is working correctly.

This work focuses on a semi-idealized DRDE simulation as described in the next section. The computational domain is confined to the space in between two circumferential planes comprising the inlet and exit (i.e. the channel region of Fig. 1). As such, no assessment is made of potential losses associated with radial-to-axial flow turning at the inner or outer diameters. Such simplification is justified due to the preliminary nature of this work, and by the stated goal of examining whether a fundamental physics based advantage exists for the radial configuration. The CFD code is first described. Several sample calculation results from relatively simple flow scenarios are then presented as validation. The performance figure of merit used in this work is then detailed. Following this, results from several converged cycle calculations are shown and compared to those from approximately equivalent annular RDE cycles computed with the same code. The results indicate that outer-to-inner diameter flow configurations produce the highest performance. It is also shown that, as with annular RDE's, reducing the exit cross-sectional area relative to the inlet improves performance compared to constant cross-sectional area. Finally, it is demonstrated that in this semi-idealized simulation environment, the DRDE performs as well or better than the annular RDE.

II. Code Description

The code used for this work is a modified version of one that has been documented and validated extensively in the literature [5-12]. It was originally developed for annular (aka, axial) RDE's and is briefly described below for that configuration. Modifications necessary for DRDE analysis are then presented.

The code is a formally high-resolution algorithm that integrates the quasi-two-dimensional, two-species, reactive Euler equations with source terms, on a regular Cartesian grid. The code adopts the detonation frame of reference and deliberately utilizes a coarse grid (i.e. adds a degree of numerical diffusion) in order to eliminate the highest frequency unsteadiness (e.g. detonation cells, Kelvin-Helmholtz phenomena, etc.). The result is a flowfield solution that is invariant with time when converged. The working fluid is assumed to be a single, calorically perfect gas with only two species: premixed reactant or product.

The source terms contain sub-models that govern the reaction rate, momentum losses due to skin-friction, and the effects of heat transfer to the walls. For this work, skin friction and heat transfer are neglected. The reaction rate sub-model is one which is proportional to the product of the rate constant, K_0, the density, ρ, and the reactant mass fraction, z. Although this form lacks a typical Arrhenius-type exponential for temperature dependence, it does utilize a user defined threshold temperature, below which the reaction is not allowed to proceed. For all of the results shown, the threshold temperature is specified as 2.5 times the reference temperature. Such a reaction model successfully captures effects within the flowfield that are germane to this work. Regions where deflagration is presumed to occur rather than detonation are user-specified by assigning a lower reaction rate constant to the cells therein.

For all results that follow, properties of premixed stoichiometric hydrogen and air are used. The relevant parameters are: a specific heat ratio, γ=1.264; a real gas constant, R_g=73.92 ft-lb_f/lb_m/R; and a fuel heating value, h_f=51,571 BTU/lb_m.

The simulation is implemented non-dimensionally. The non-dimensional pressure, p, density, ρ, temperature, T, and velocities, u and v are obtained by normalizing to a reference state which for this work is: p^*=14.7 psia, ρ^*=0.055 lb_m/ft^3, T^*=520 R, and the corresponding sound speed, a^*=1250 ft/s. The azimuthal and axial directions, x and y are non-dimensionalized by the annular circumference at the mean diameter, l. The time, t, is non-dimensionalized using the reference wave transit time, l/a^*. Unless stated otherwise, all quantities displayed or discussed henceforth are non-dimensional. For reference, it is noted that this formulation results in an equation of state that is as follows.

$$p = \rho T \tag{1}$$

The speed of sound is

$$a = \sqrt{T} \tag{2}$$

The governing equations are integrated numerically in time using an explicit, second-order, two-step, Runge-Kutta technique. Spatial flux derivatives are approximated as flux differences, with the fluxes at the discrete cell faces evaluated using Roe's approximate Riemann solver. Second-order spatial accuracy (away from discontinuities) is obtained using piecewise linear representation of the primitive variable states within the cells (MUSCL). Oscillatory behavior is avoided by limiting the linear slopes.

With reference to the Fig. 2 annular RDE computational space, the following boundary conditions are imposed. At x=0.0 and x=1.0, periodic (aka symmetric) conditions are used. These ensure that the x-dimension of the computational space correctly represents an annulus (which is continuous and has no boundary). At y=y_{max}, constant pressure outflow is imposed along with characteristic equations to obtain ρ and v for the image cells. If the resulting flow is sonic, or supersonic, then the imposed pressure is disregarded. If, in addition, the upstream flow is supersonic, then p, ρ, and v are extrapolated from the interior. The possibility for a normal shock solution whereby supersonic outflow jumps to subsonic is also accommodated. The x-velocity component u is extrapolated from the interior at each boundary location. At y=0.0 (the inflow face), partially open boundary conditions are applied [8]. This face is presumably fed by a large manifold at a fixed total pressure, and temperature. The manifold terminates at the face and is separated from it via an orifice. The ratio of orifice flow area to RDE annulus area, A_i/A_{ch} is generally less than 1. If the interior pressure is less than the manifold pressure, p_m, then inflow occurs. The boundary condition routine determines p, ρ, and v for the inflow face image cells subject to a momentum (total pressure) loss model which depends on the mass flow rate and the value of A_i/A_{ch}. The routine is capable of accommodating a scenario where the inflow becomes choked. If A_i/A_{ch} = 1, the inlet is lossless. The x-velocity component u is prescribed during inflow, and it is here that a reference frame change is implemented. Rather than specify u=0 (i.e. no swirl) which is the laboratory or fixed frame condition, the negative of the detonation speed, u_{det} is prescribed instead. As a result of this change to the detonation reference frame, the computational space becomes one where a steady-state solution is possible. If the interior pressure along the inlet face is greater than P_m, as might be found just behind the detonation, then there will be backflow into the manifold through the orifice. The boundary condition routine normally accommodates this as well. However, for this work a notional check-valve boundary condition is implemented which detects when backflow should occur, and applies a solid wall boundary condition.

A. Modifications for the DRDE Configuration

Modifying the annular RDE code for the DRDE configuration entailed only minor changes to the interior numerical approach; however, changes to boundary conditions were extensive. The interior changes were twofold. First, the length scale used for non-dimensionalization was changed from the annular circumference l, to the outer diameter, D_o. Second, and more critical, was a shift from the detonation frame of reference to that of the laboratory. This, in turn meant abandoning the fixed spatial regions for deflagration and detonation. The frame of reference

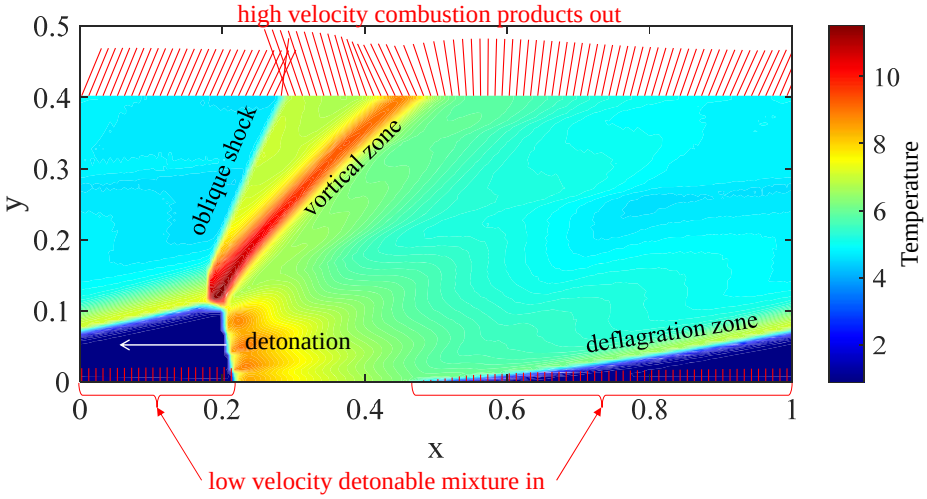

Fig. 2 Typical converged annular RDE flowfield shown as contours of non-dimensional temperature. Scaled inlet and outlet plane velocity vectors are also shown in red.

change was necessary since in the DRDE, the detonation is constantly changing direction as it rotates. This makes the detonation frame of reference an accelerating one which cannot be accommodated within the framework of the governing equations. It was found that adding a simple pressure threshold to the reaction equation was sufficient to distinguish between deflagration and detonation zones. If the pressure in a numerical cell was more than twice the manifold pressure (and the temperature was above the threshold), then the detonative rate constant was used. Otherwise, the deflagrative rate constant was used. This change was tested in an annular RDE simulation that had originally converged in the detonation frame of reference. The imposed circumferential detonation velocity at the inlet was set to 0.0. The pressure threshold just described was imposed on the reaction equations, and the fixed spatial detonation/deflagration regions were removed. The resulting simulation produced nearly the exact same solution as the detonation frame, except that it propagated to the left (see Fig. 2) at the detonation speed.

As mentioned, boundary condition modifications for the DRDE configuration were extensive. Figure 3 illustrates a 50 X 50 cell grid encompassing a device with an inner to outer diameter ratio of D_i/D_o=0.4. Ghost cells, where boundary conditions need to be applied, are marked with a '+' for those corresponding to the y direction and a '·' for those in the x direction. Interior cells are shown as green squares. Excluded cells where no computations are performed are shown as white squares. It is evident that the circular boundaries are approximated by a combination of vertical and horizontal faces. This implies that inflow, outflow, and wall boundary conditions must be implemented in both the vertical and horizontal directions, at any of the boundary cells shown. This contrasts with the annular RDE configuration where inflow and/or wall boundary conditions are in a single plane along y=0.0 and occur only in the vertical dimension. Similarly, annular RDE outflow occurs only along the $y=y_{max}$ plane.

Additionally, for inflow boundary conditions the DRDE configuration requires that the flow direction is purely radial. Considering the Fig. 3 geometry, and noting the Cartesian coordinate system, it is clear that requiring flow to travel radially (and isentropically) from a manifold at either the inner or outer diameter boundary into the DRDE significantly complicates the inflow algorithm. The algorithm is an iterative one that simultaneously solves for the characteristic waves between the ghost and adjacent interior cells, and the isentropic flow assumed between the manifold and ghost cells (with the possibility of momentum loss if A_i/A_{ch}<1.0) [13]. The iteration parameter is the static pressure at the inlet throat. For each iteration, the static pressure is used to obtain the manifold velocity component. In the DRDE this velocity is then resolved into its x and y components in order to complete an iteration. In the annular RDE configuration where inflow occurs only in the y-direction (and along a single plane), no component resolution is necessary. Fortunately, these boundary complications are predominantly algebraic and trigonometric, and as such require relatively straightforward modifications to accommodate. The sample calculations which follow serve as proof that the accommodations were done correctly.

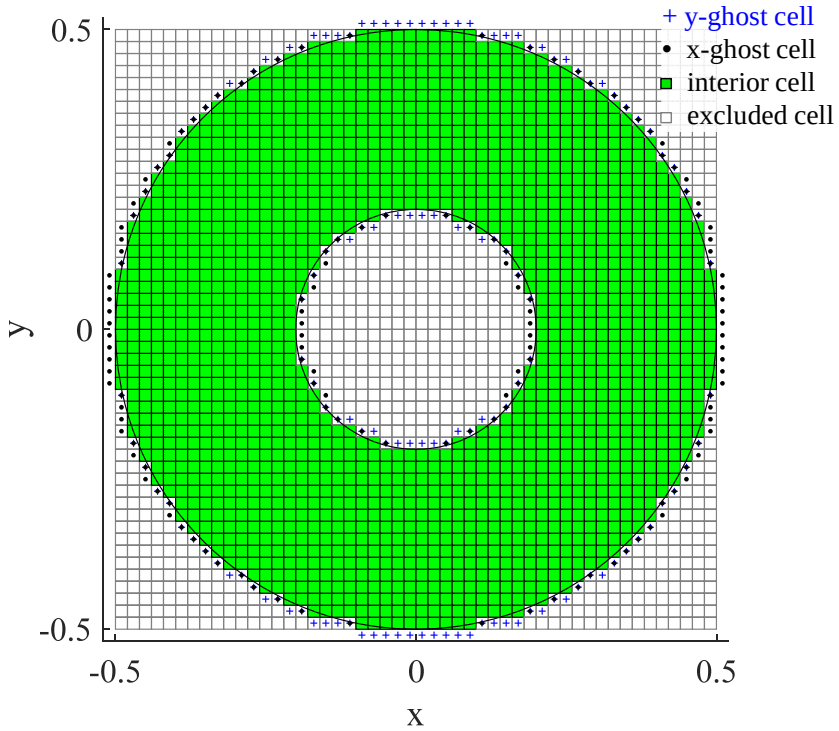

Fig. 3 50 X 50 DRDE Cartesian grid showing boundary, or ghost cells, and interior cells.

Implementation of an inlet check-valve to prevent backflow (i.e. a solid wall boundary condition) also required modification. In the annular RDE wall boundary conditions are only required in the y=0.0 plane. Values are assigned to the ghost cells which ensure that the normal velocity component in this plane, v, is zero. This is achieved by setting the ghost cell normal velocity to the negative value of the nearest interior cell. The pressure, density, and tangential velocity component, u, of the ghost cell are set identical to the nearest interior cell. In the DRDE configuration, the velocity components normal and tangential to the wall are found by

projecting the nearest interior values of u and v on to the normal and tangential unit vectors associated with the circular boundary at a given location [14]. As with the inflow boundary conditions, the projection process is a straightforward application of trigonometry.

B. Simple Tests

Figure 4 shows contours of pressure at two different times during a non-reactive, radial inflow test whereby a quiescent fluid is induced into motion by a shock wave. The initial conditions at t=0.0 are p, ρ, u, v, z = 1, 1, 0, 0, 0. The inner diameter exit boundary is a constant pressure surface held at p_{exit}=1.0. The manifold at the outer diameter inflow boundary is held at a constant total state of p_m=2.0, T_m=1.038. The ratio of inner to outer diameter is D_i/D_o=0.5. The ratio of inlet to channel cross-sectional area is A_i/A_{ch}=1.0. For this and all subsequent simulation results, the grid is 200 X 200 cells. The left contour plot corresponds to t=0.1. Here it is shown that a shock is propagating radially inward through the quiescent fluid and has reached approximately $0.742D_o$. This is precisely the distance that a shock of this strength should have traveled according to theory [15]. The right hand contour plot corresponds to t=1.2. By this time the original shock has reflected between the inner and outer boundaries many times and the flow has reached steady state. The radial gradient in pressure is appropriate since the constant channel height profile creates a reduction in area as the flow travels inward (i.e. the Fig. 4 configuration represents a radial converging nozzle). As such, and though not shown, the exit (inner diameter) flow is choked. Also shown in both of the Fig. 4 contour plots are some of the boundary velocity vectors (in green). It is clear that the flow is radial and circumferentially uniform, as expected. The respective lengths of the inflow and outflow vectors of the right hand contour are correct for the radially converging nozzle. Finally, it is confirmed that at t=1.2 the mass flow rate into the disk at D_o matches the flow rate out at D_i. These results suggest that the boundary condition modifications made to the code and described above are working correctly. It is noted but not shown that a similar test was conducted for a non-reacting, radial outflow configuration. The results provided a similarly favorable comparison.

Figure 5 shows contours of temperature at two different times during the simulation of a single detonation event propagating through a quiescent, detonable mixture, in a disk configuration with a cross-sectional area shown in the center of the figure. There are solid walls at the inner and outer radius. The initial conditions at t=0.0 are p, ρ, u, v, z = 1, 1, 0, 0, 1 everywhere except the small square region shown at the bottom of the left contour where p, ρ, u, v, z = 17, 1.75, 0, 0, 0. This high pressure, high temperature, post-reactive region initiates the detonation. The right hand contour plot shows the state at t=0.205. Two curved and symmetric detonation fronts are seen propagating in opposite directions around the disk. Behind each detonation is a strong, curved oblique shock which appears to be a reflection from the outer wall. Also shown in the right hand contour plot are velocity vectors (in green) for one of the detonation fronts at points where the reaction is 70-75% complete. It is evident that the fluid is not traveling in a purely circumferential direction and must subsequently be turned. The theoretical one-dimensional detonation speed (aka, the Chapman-Jouguet or CJ speed) for this reactant combination is u_{det}=5.47. The measured circumferential detonation propagation speed at the inner diameter is 4.0. At the outer diameter it is 7.58. At the average of the inner

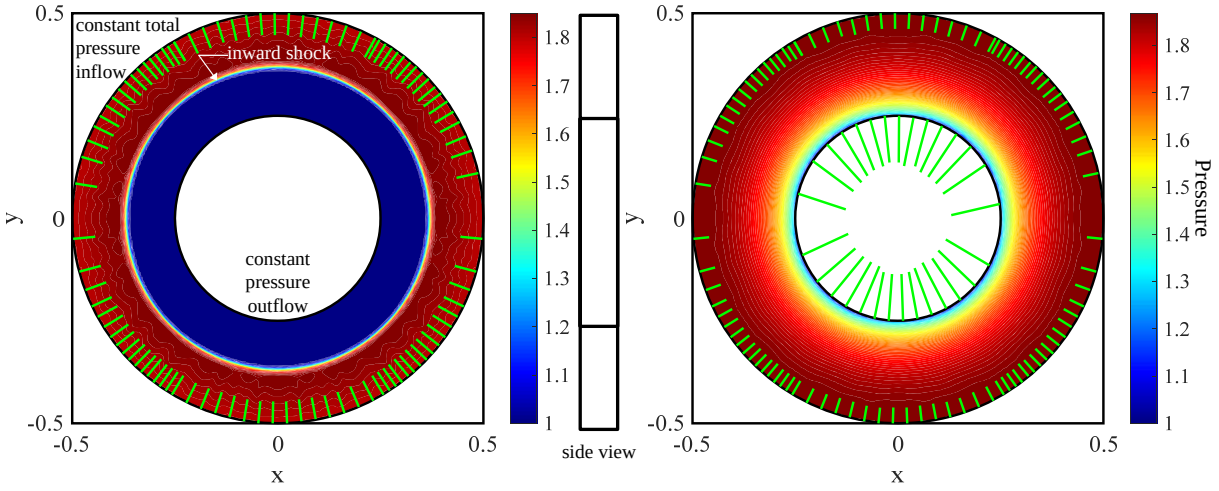

Fig. 4 Contours of pressure at t=0.1 (left) and t=1.2 (right) during shock induced radial inflow with constant pressure at D_i and constant total pressure at D_o, and with the cross-sectional profile shown (center). Some boundary velocity vectors are shown in green.

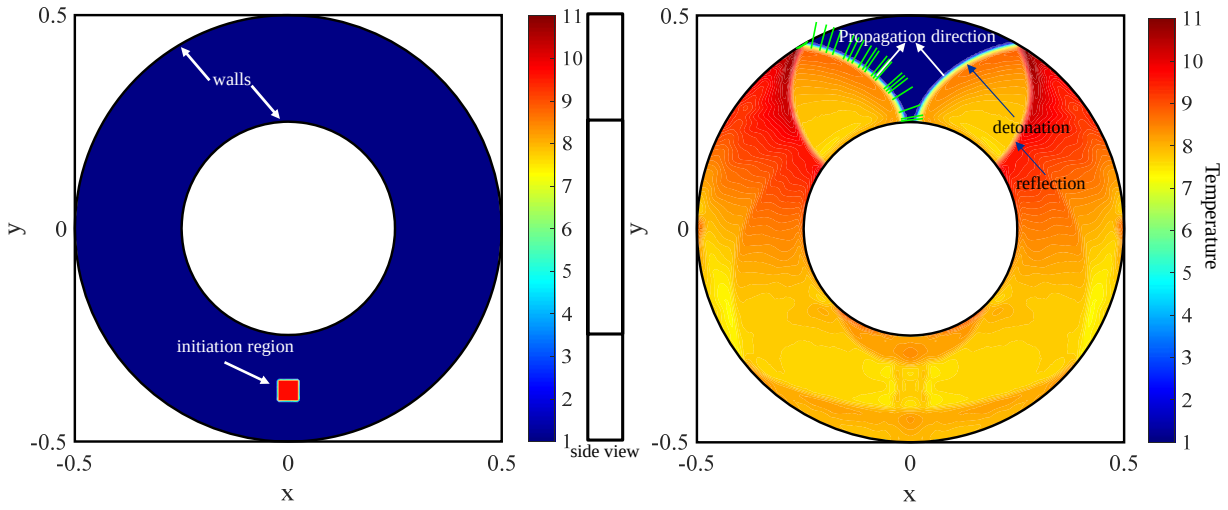

Fig. 5 Contours of temperature at t=0 (left) and t=0.205 (right) during the symmetric propagation of two detonation waves around a disk with walls at D_i and D_o, and with the cross-sectional profile shown (center). Velocity vectors are shown in green in the right hand contour for one of the detonation fronts at the point where the reaction is 70-75% complete.

and outer diameters it is 5.87. This is a somewhat intuitive result since the speed of the detonation is governed by the strength of the associated shock wave. The shock wave at the outer diameter is stronger because it is oblique to a concave wall. At the inner diameter it is oblique to a convex wall and is therefore weaker.

While it cannot be stated that the Fig. 5 results represent validation of the wall boundary condition and interior numerical scheme modifications, they do indicate that both are performing consistently and as expected. Since there is no analytically solvable flowfield for the DRDE configuration with which to compare the code, consistency and meeting expectations are the only validation available. It is noted as well that the detonation structure shown in Fig. 5 is quite similar to that described analytically and experimentally in Ref. 16.

III. Results and Discussion

All of the DRDE results shown utilize an inlet manifold state of p_m=4.0, T_m=1.038 and an exit boundary pressure of p_{exit}=1.0. The idealized inlet 'check-valve' is utilized so that backflow into the inlet behind the detonation is prevented. Presentation of results necessarily includes measurement of engine performance, as described below.

A. Figure of Merit

The radial and circumferential nature of the DRDE exit flow makes the use of ideal exhaust Equivalent Available Pressure (EAP_i) [17, 18] difficult to evaluate in a Cartesian system, and possibly dubious as a figure of merit in this configuration. In this work an exit plane Entropy Equivalent Pressure, *EEP* is used instead. *EEP* is defined here as the total pressure, at the mass-flux averaged exit total temperature, required to produce the mass-flux averaged entropy.

For reference, the mass flux-average of any quantity φ (denoted with an overbar) is defined as follows.

$$\overline{\varphi} = \frac{\sum_{k=1}^{t_{cycle}/t_{output}} \left[\sum_{i,j=exit} \varphi_{i,j} \rho_{i,j} U^n_{i,j} \right]_k}{\sum_{k=1}^{t_{cycle}/t_{output}} \left[\sum_{i,j=exit} \rho_{i,j} U^n_{i,j} \right]_k} \tag{3}$$

Here, the subscripts *i* and *j* refer to indices associated with numerical cells having a face at the exit boundary. The term U^n represent the cell velocity component (*u* or *v*) which is normal to the boundary face. As is clear from Fig. 2, either an inner or an outer diameter boundary is comprised of both horizontal and vertical faces. The second summation in Eq. 3 (associated with the temporal index *k*) requires a limit cycle. The limit cycle is one where the computational state repeats itself each wave revolution. In this Cartesian system, it is found that the summation of fluxes at the boundaries varies slightly depending on the angular position of the detonation, even after a limit cycle is

established. As such, the limit cycle period is divided into 50 time intervals. At each time interval the spatial boundary flux summations of Eq. 3 are evaluated (over *i* and *j*). When the cycle is complete the 50 summations are themselves summed (over *k*) to complete the mass flux-average.

The entropy is defined as

$$s = \frac{\gamma}{(\gamma - 1)} ln(T) - ln(p) \tag{4}$$

The total temperature is

$$T_t = T + \frac{(\gamma - 1)}{2}\left[u^2 + v^2\right] \tag{6}$$

The exit flow *EEP* is then

$$EEP = \overline{T}_t^{\frac{\gamma}{\gamma-1}} e^{-\overline{s}} \tag{7}$$

EEP generally yields higher values than EAP_i. This is because the former is based on an assumption that all components of the exhausting velocity contribute to availability for thrust or work production, while the latter is based on an arguably more realistic assumption that only velocity components normal to the exit plane contribute. The disparity between the two gets larger as the RDE length (or DRDE radial extent) is reduced. With reference to the Fig. 2 exit velocity vectors, it is clear that RDE's have significant non-normal components. The closer to the top of the detonation that this exit plane is, the larger the non-normal components. Nevertheless, EEP is straightforward to calculate and is an effective means of comparing the relative performance of various configurations.

B. Ideal Operation: A_i/A_{ch}=1.0 with Constant Cross-Sectional Area

The first configuration examined was considered to be the disk equivalent to the most basic annular RDE. This means there was no restriction on the inlet (A_i/A_{ch}=1.0), making it lossless, and the cross-sectional area was constant. The ratio of inner to outer diameter was set to D_i/D_o=0.4. This value correspond roughly to the minimum axial length to circumference ratio in an annular RDE (i.e. an RDE of length y=0.136 in Fig. 2) that contains the full detonation height with no fueled mixture spillage, and results in choked exit flow. The disk channel height profile is shown in Fig. 6.

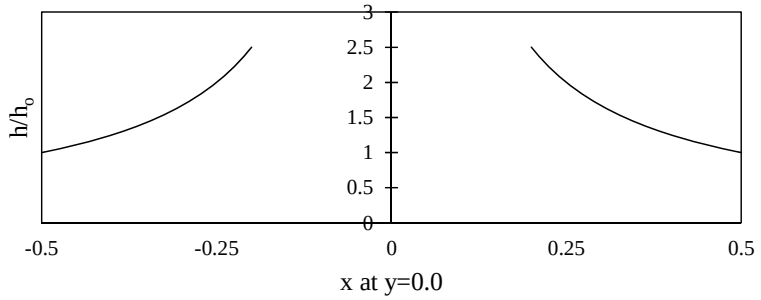

Fig. 6 DRDE height profile.

Interestingly, this idealized scenario proved unstable for either inward or outward flow configurations. Figure 7 shows contour plots of temperature at four successive revolutions of the detonation, beginning approximately 5 revolutions after the simulation was initiated, for an inward flowing configuration. These contours contrast with the left hand contour of Fig. 1 which shows a stable configuration that will be more fully explored in Section 3C. It is shown in Fig. 7 that the interface between the fresh and reacted mixture becomes more distorted with each revolution. Left to run indefinitely, the distortion amplifies until the detonation ultimately fails. This behavior is reminiscent of the instability described for an annular RDE with an exhaust throat restriction [12], though it is not certain that the same mechanism is at work. This is not a particularly realistic configuration, so no more study was undertaken. It is simply worth noting that an annular RDE running this same basic ideal configuration is stable. This suggests that the DRDE configuration gives rise to some fundamentally different fluidic processes.

Contour plots of temperature are shown in Fig. 8 at four successive revolutions of the detonation, beginning approximately 5 revolutions after the simulation was initiated, for an outward flowing configuration. These contours should be contrasted with the right hand contour of Fig. 1. It is seen that the detonation height is low on the first

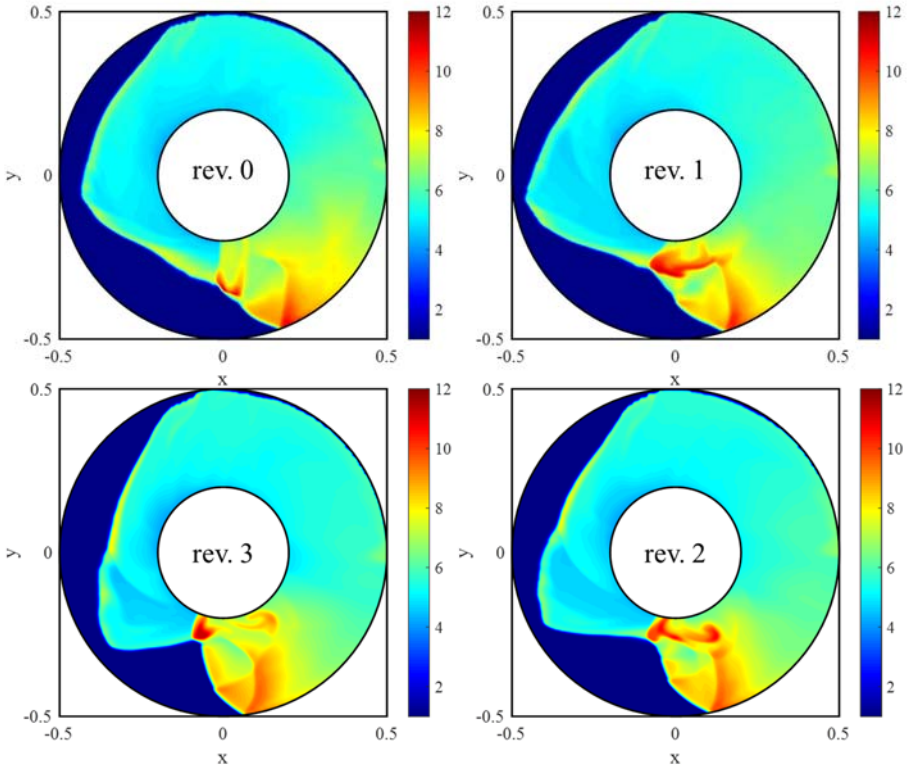

Fig. 7 Contours of temperature at four successive detonation revolutions of a radially inward flowing DRDE with constant cross-sectional area and A_i/A_{ch}=1.0.

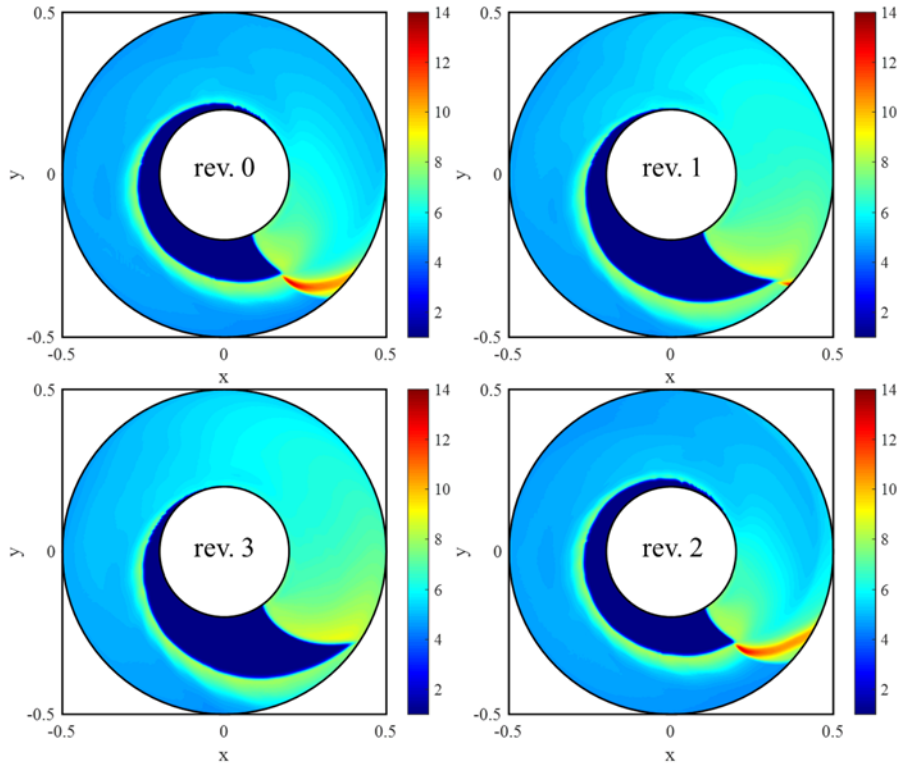

Fig. 8 Contours of temperature at four successive detonation revolutions of a radially outward flowing DRDE with constant cross-sectional area and A_i/A_{ch}=1.0.

revolution (rev. 0), large on the second, even smaller on the third, and even larger on the fourth. Given enough revolutions, this sort of 'rotational eccentricity' grows until the detonation height ultimately exceeds the outer diameter and unreacted mixture exits the device. Since this is an unacceptable situation, the simulation was stopped. It is not clear why this behavior occurs; however, it was only observed in this idealized configuration, so further study was not pursued. The results are shown here only to highlight again that DRDE flowfields are fundamentally different than those of annular RDE's.

C. Stable Operation: A_i/A_{ch}=0.6 with Constant Cross-Sectional Area

Using an inlet restriction of A_i/A_{ch}=0.6, along with the same D_i/D_o=0.4 and Fig. 6 height profile as the previous tests resulted in stable, limit cycle operation. The addition of an inlet restriction, with its associated aerodynamic loss, also resulted in a simulation which was a modestly closer approximation to an actual DRDE. The particular value of 0.6 was chosen as an estimate of that which would produce minimal loss to inflow and adequate resistance to backflow in an actual RDE inlet without the notional check-valve used for this work. A value of A_i/A_{ch}=0.6 was also found to yield peak performance in Ref. 12. Contour plots of temperature and Log(pressure) at a moment in time after 10 wave revolutions are shown in Fig. 9 for the inward flow configuration. Also shown in green at the boundaries are velocity vectors indicating magnitude and direction. It is interesting to note that the detonation profile is similar to that of Fig. 5, except that it is truncated. Analogous to Fig. 2, it is observed that little of the exiting flow is purely radial even though all of the incoming flow is. As with annular RDE's however, it is noted that the mass-flux averaged circumferential velocity is zero (i.e. no net swirl), as mandated by the governing equations of motion [5]. This type of exit flow field could present a challenge for downstream work extraction turbine guide vanes, or for a thrust producing nozzle. This is because any type of flow guiding surface will see large changes of incidence combined with relatively high velocities that are difficult to direct. The detonation speed based on the circumferential propagation rate at D_o is approximately 24% above the theoretical CJ speed. Summations of mass and enthalpy fluxes at the boundaries verify that mass and energy are conserved to within 1% for this and all results presented. Pressure gain in this work is defined as

$$PG = \frac{EEP}{P_m} - 1.0 \tag{8}$$

It is found that PG=90% for this configuration. This compares to PG=71% for an annular RDE of axial length y=0.136 (see Fig. 2) using the same boundary conditions, A_i/A_{ch}, and constant cross-sectional area. The reasons for this nearly 20% improvement are unclear as of this preliminary work; however, one possibility is the aforementioned detonation shock wave being oblique to a concave wall. This means that the flow behind the shock turns in order to follow the wall. The flow is turned by a pressure rise at the location where heat is being released in the narrow detonation

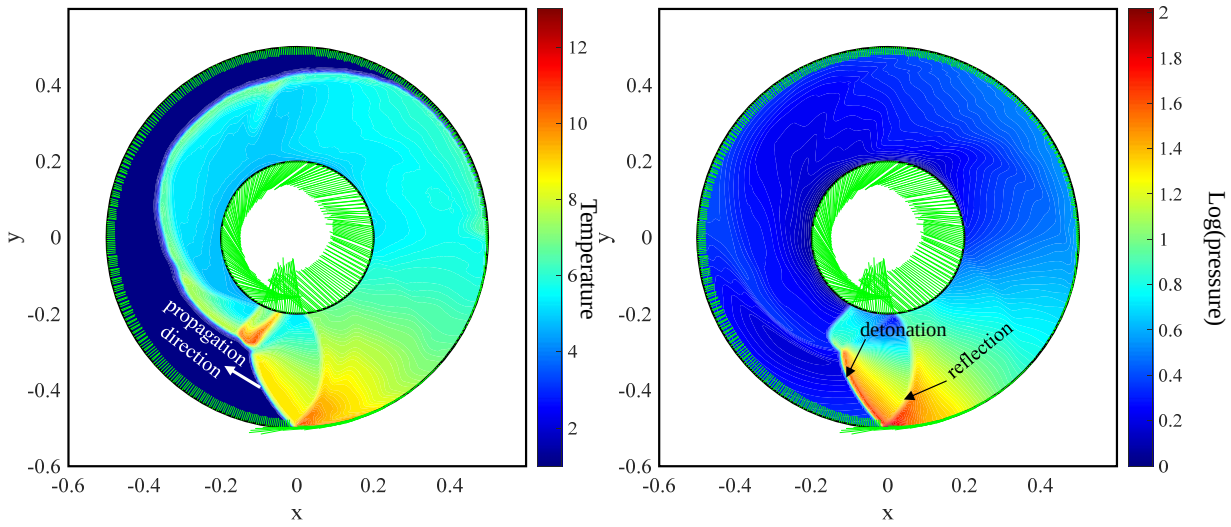

Fig. 9 Contours of temperature (left) and Log(pressure) (right), with superimposed velocity vectors, during limit cycle operation of a radially inward flowing DRDE with A_i/A_{ch}=0.6, D_i/D_o=0.4, and constant cross-sectional area.

reaction zone. Heat addition at higher pressure than an annular RDE, which does not exhibit this flow turning, should yield better performance.

Figure 10 shows the same information as Fig. 9 for the outward flow configuration under the same conditions. The mass flux rate through this configuration is approximately 11% less that the inflow version. The detonation speed based on the circumferential propagation rate at D_i is 35% below the CJ value. Interestingly, the operational frequency for the same size device as Fig. 9 is 30% higher even though the detonation speed is lower. The pressure gain is PG=65%, which is lower than the equivalent annular RDE. This result is consistent with the flow turning described earlier since in this outward configuration the flow is turned around a concave surface at the detonation shock, which drops the pressure in the detonation reaction zone. Note that the pressure color scales are the same in Figs. 9 and 10, and it is clear that the pressure behind the detonation shock is higher in Fig. 9, particularly near where the wall meets the detonation.

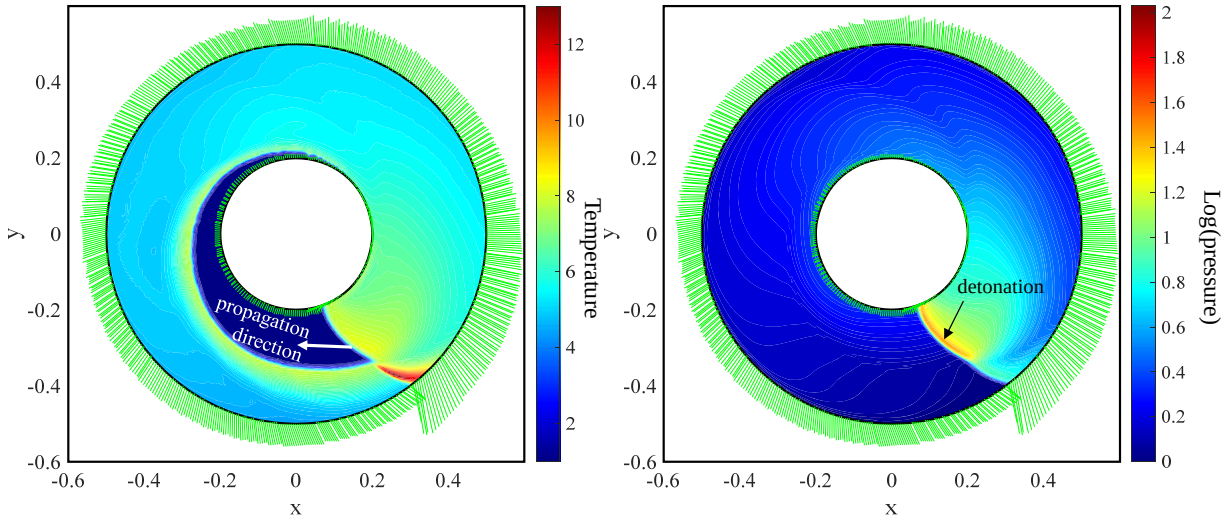

Fig. 10 Contours of temperature (left) and Log(pressure) (right), with superimposed velocity vectors, during limit cycle operation of a radially outward flowing DRDE with A_i/A_{ch}=0.6, D_i/D_o=0.4, and constant cross-sectional area.

D. Diameter Ratio Reduction

The simulation configurations from Section III C were modified to have D_i/D_o=0.3. Both the inward and outward flowing were run until a limit cycle was achieved. Figure 11 shows contour plots of temperature, and boundary velocity vectors for the inward (left) and outward (right) configurations, at a moment in time. The performance parameters are listed in Table 1 along with those from Section III C. Here it is seen that for D_i/D_o=0.3, the annular RDE has the best performance compared to either DRDE configuration. The annular RDE shows a slight decrease in performance (-3%) as its length is increased. This is because the circumferential velocity components are continually dissipated by the oblique shock and vortical zone of Fig. 2, and dissipative processes produce entropy. The outward flowing DRDE shows a much larger performance reduction (-11%) as its radial length is increased. This could be due to a similar mechanism as the annular RDE, though it is not obvious why it causes so much more loss in performance. The inward flowing DRDE shows a profound performance loss (-24%) as the radial length is increased (D_i/D_o is reduced). Investigation beyond this preliminary assessment is needed to determine the reason for this sensitivity. However, it is observed that the high entropy vortical portion of the flowfield (see left contour of Fig. 11) becomes significantly enlarged as the diameter ratio is reduced. This high entropy structure passes over, or 'processes' a significant fraction of throughflow mass. It is possible that the explanation for the performance reduction therefore lies in understanding this portion of the flowfield. For the goals of the present work it is concluded that reducing diameter ratio degrades performance for either inward or outward DRDE configurations.

Table 1 Simulation Performance Parameters With A_i/A_{ch}=0.6

	D_i/D_o=0.3		D_i/D_o=0.4	
Configuration	**Det. Speed (% from CJ)**	**PG (%)**	**Det. Speed (% from CJ)**	**PG (%)**
Inward	***+43***	***+66***	***+24***	***+90***
Outward	***-39***	***+54***	***-35***	***+65***
Annular*	***-14***	***+68***	***-15***	***+71***

**Annular equivalent axial lengths are y=0.171 and 0.136*

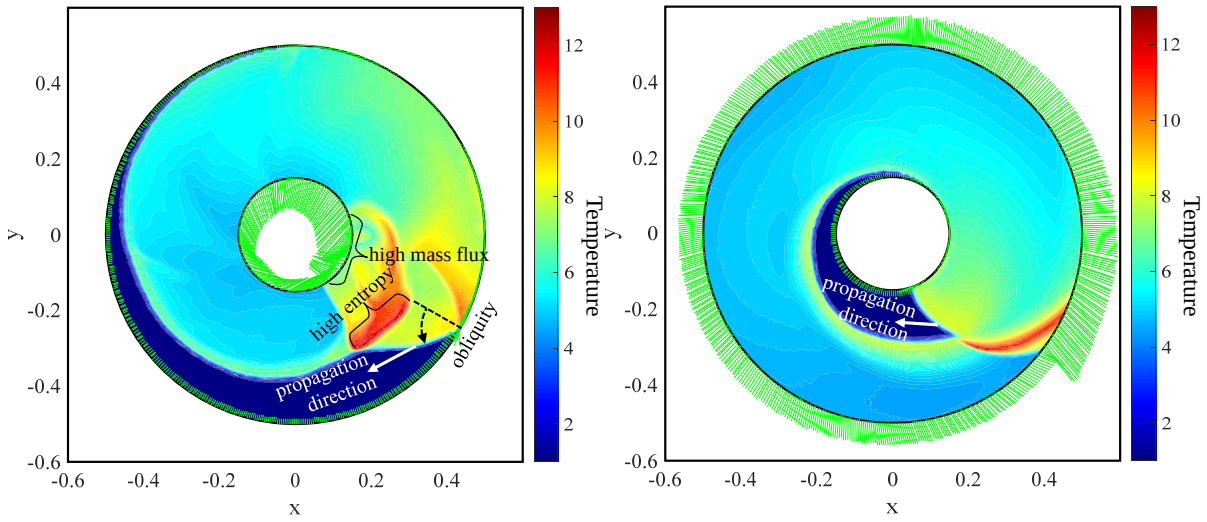

Fig. 11 Contours of temperature, with superimposed velocity vectors, during limit cycle operation of an inward flowing (left), and an outward flowing (right) DRDE with A_i/A_{ch}=0.6, D_i/D_o=0.3, and constant cross-sectional area.

It is interesting to observe that for the inward flow configuration, the angle of obliquity shown on the left contour plot of Fig. 11 increases from approximately 40 degrees for D_i/D_o=0.4 to 50 degrees here. It is unclear why this increase occurs, or if it impacts performance. It is noted however, that the increased obliquity is also associated with a higher apparent detonation speed. This is likely because the 'detonation speed' being measured is the rate at which the intersection wave and the outer wall propagate around the circumference. On a concave wall, this is higher than the rate at which each point of the wave is propagating through the fluid (see detonation velocity vectors in Fig. 5). And the disparity increases with the degree of obliquity.

E. Outflow-to-Inflow Plane Cross-Sectional Area Ratio Reduction

Studies have shown that an exit throat (i.e. A_{exit}/A_{ch}<1.0) leads to improved performance relative to constant cross-sectional area in annular RDE's [8, 12]. The exit restriction reduces the fill Mach number, and raises the pre-detonation pressure. Both effects raise the pressure after the reaction and thus increase availability. A limited test of whether this held true for the DRDE was executed for both the inward and outward flow configurations. An inlet restriction of A_i/A_{ch}=0.6 was used along with a diameter ratio of D_i/D_o=0.4. The cross-sectional area was reduced linearly with radius by 30% from the inlet diameter to the exit diameter. The channel height profiles for the two configurations are shown in Fig. 12. Limit cycle temperature contour plots similar to Fig. 11 are shown for each configuration in Fig. 13. As expected, the detonation height is reduced for both configurations in comparison with constant cross-sectional area simulations. Performance parameters are shown in Table 2 along with those from the right hand side of Table 1 (constant cross-sectional area) for comparison. The pressure gain is observed to increase when a throat is added for both of the DRDE configurations. That associated with the inward flow configuration is increased by a remarkable 52%. Again it is shown that the inward flow configuration outperforms both the outward flow configuration of the DRDE and the annular RDE. It is noted that the left contour plot of Fig. 12 has the same enlarged, high entropy region as was pointed out in Fig. 11, yet it still results in a high performance configuration.

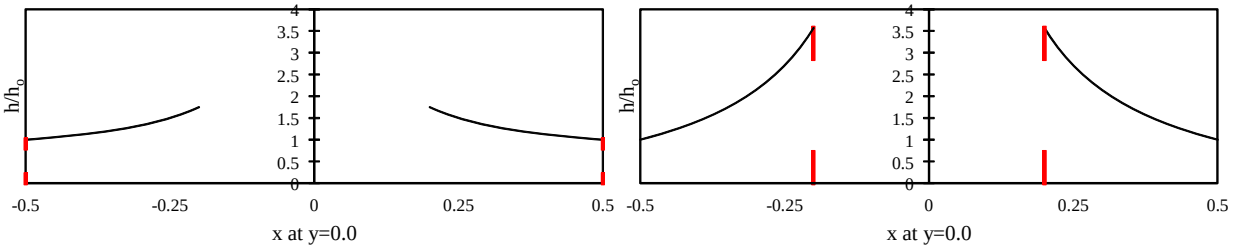

Fig. 12 Height profiles for the inward flowing (left), and outward flowing (right) DRDE's with A_i/A_{ch}=0.6, D_i/D_o=0.4, and a linearly varying cross-sectional area reduction of 30% from inlet to exit. The inlet restriction is shown in red.

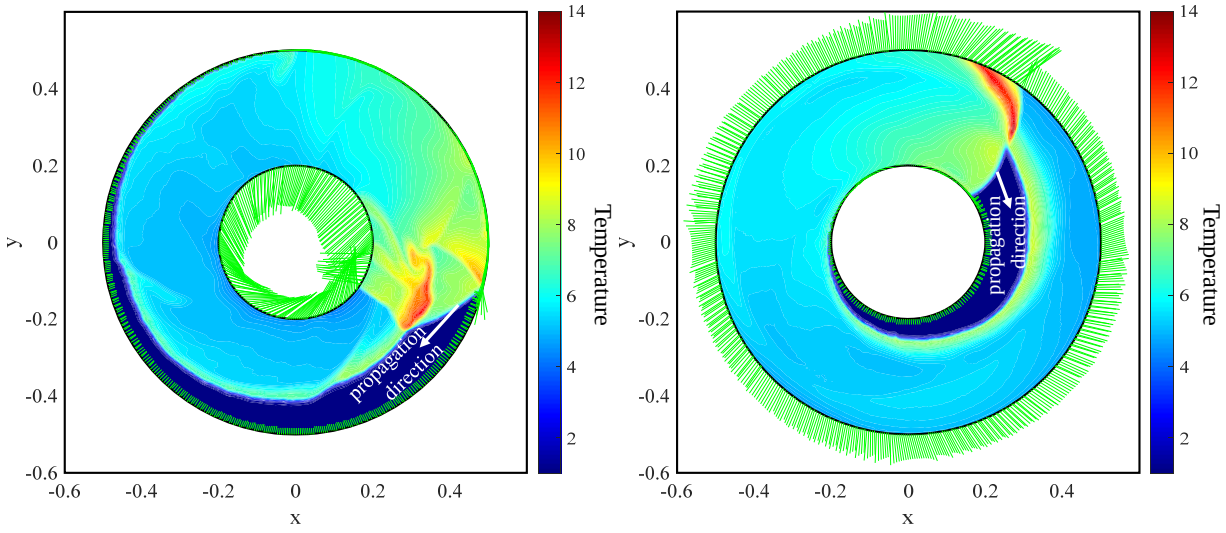

Fig. 13 Contours of temperature, with superimposed velocity vectors, during limit cycle operation of a radially inward flowing (left), and a radially outward flowing (right) DRDE with A_i/A_{ch}=0.6, D_i/D_o=0.4, and a linear cross-sectional area reduction of 30% from inlet to exit.

Table 2 Simulation Performance Parameters With A_i/A_{ch}=0.6

	A_{exit}/A_{ch}=0.7		A_{exit}/A_{ch}=1.0	
Configuration	**Det. Speed (% from CJ)**	**PG (%)**	**Det. Speed (% from CJ)**	**PG (%)**
Inward	***+27***	***+142***	***+24***	***+90***
Outward	***-34***	***+105***	***-35***	***+65***
Annular*	***-14***	***+140***	***-15***	***+71***

**The annular RDE area variation is not linear. It is similar to the exit throat described in Ref. 12*

This suggests that the benefits of area restriction outweigh the as yet unquantified decrements associated with this region.

Reducing the exit area further to A_{exit}/A_{ch}=0.6 resulted in unstable flow similar to Fig. 7 for the inward flow configuration. For the outward flow configuration, it produced a stable limit cycle and an associated pressure gain of PG=148%. This is the highest value of pressure gain observed; however, there is some uncertainty regarding the result. The channel height profile for this simulation contains even larger spatial gradients than the right hand side of Fig. 12 (the inner diameter height is h/h_o=4.17) which calls into question the validity of the quasi-two-dimensional assumption of the present simulation. It is also worth noting that flow traveling radially outward may be particularly challenging to extract work from via a turbine, or to turn axially in order to obtain thrust. Nevertheless, the high pressure gain achieved certainly warrants further exploration. Further exit area restriction to A_{exit}/A_{ch}=0.5 also produced stable results; however, the pressure gain dropped to PG=143%. As such, and in keeping with the preliminary nature of this work, no further restriction was examined.

IV. Conclusions

A disk rotating detonation engine (DRDE) has been described where the working fluid enters and exits in a predominantly radial manner. Two configurations were considered, one where the flow direction was radially inward and the other where it was radially outward. The configurations were examined using a validated, quasi-two-dimensional, premixed, reacting computational fluid dynamic simulation, originally developed to examine the physics and performance of annular RDE's, and modified to accommodate the radial and circumferential DRDE flowfields. The simulation was executed in a semi-idealized mode such that it was adiabatic, inviscid, and did not allow backflow at the inlet. Variations in flow direction, inner-to-outer diameter ratio, inner-to-outer cross-sectional area ratio, and inlet throat-to-channel area ratio were examined using an entropy-based measure of pressure gain as a figure of merit. It was found that the inward flowing DRDE outperformed the outward flowing configuration if other parameters were the same. The inward flowing DRDE was further shown to outperform the equivalent annular RDE. These results, though preliminary, demonstrate the potential of the DRDE configuration, and provide motivation for additional investigation.

Acknowledgements

This work was made possible, in part, by a Reimbursable Space Act Agreement between the NASA Glenn Research Center and the Air Force Research Laboratory, in Dayton Ohio (SAA3-1325-40). The author gratefully acknowledges the support.

References

[1] Ishiyama, C., et al, "Experimental Study of Research of Centrifugal-Compressor-Radial-Turbine Type Rotating Detonation Engine," AIAA-2016-5103, July, 2016.
[2] Higashi, J., et al, "Experimental Study of Disk-Shaped Rotating Detonation Turbine Engine," AIAA-2017-1286, January, 2017.
[3] Huff, R. T., et al, "A Radial Rotating Detonation Engine Driven Bleed Air Turbine," AIAA-2018-4879, January, 2018.
[4] Boller, S. A., et al, "Experimental Flow Visualization in a Radial Rotating Detonation Engine," AIAA-2019-1253, January, 2019.
[5] Paxson, D.E., "Numerical Analysis of a Rotating Detonation Engine in the Relative Reference Frame," AIAA-2014-0284, January, 2014, also NASA/TM 2014-216634, 2014.
[6] Paxson, D. E., Fotia, M. L., Hoke, J. L., Schauer, F. R., "Comparison of Numerically Simulated and Experimentally Measured Performance of a Rotating Detonation Engine," AIAA-2015-1101, Jan. 2015, also NASA/TM—2015-218835, 2015.
[7] Rankin, B., Fotia, M. L., Paxson, D. E., Hoke, J. L., Schauer, F. R., "Experimental and Numerical Evaluation of Pressure Gain Combustion in a Rotating Detonation Engine," AIAA-2015-0877, January, 2015.
[8] Paxson, D. E. "Impact of an Exhaust Throat on Semi-Idealized Rotating Detonation Engine Performance," AIAA-2016-1647, January, 2016, also NASA/TM-2016-219076, 2016.
[9] Theuerkauf, S. W., Schauer, F. R., Anthony, R. J., Paxson, D. E., Stevens, C. A. Hoke, J. L., "Comparison of Simulated and Measured Instantaneous Heat Flux in a Rotating Detonation Engine," AIAA 2016-1200, January, 2016.
[10] Paxson, D. E., Naples, A. "Numerical and Analytical Assessment of a Coupled Rotating Detonation Engine and Turbine Experiment," AIAA-2017-1746, January, 2017.
[11] Paxson, D. E., "Examination of Wave Speed in Rotating Detonation Engines Using Simplified Computational Fluid Dynamics," AIAA-2018-1883, January, 2018.
[12] Paxson, D. E., Schwer, D. A., "Operational Stability Limits in Rotating Detonation Engine Numerical Simulations," AIAA-2019-0748, January, 2019.
[13] Paxson, D.E., "An Improved Numerical Model for Wave Rotor Design and Analysis," AIAA-93-0482, January, 1993.
[14] Farooq M.A., Skoien, A.A., Müller B., "Cartesian Grid Method for the Compressible Euler Equations Using Simplified Ghost Point Treatments at Embedded Boundaries," *Computers and Fluids*, Elsevier, V. 82, pp. 50-62, 2013.
[15] Thompson, P. A., Compressible Fluid Dynamics, McGraw-Hill, New York, pp. 323, 1988.
[16] Nakayama, H., et al, "Stable Detonation Wave Propagation in Rectangular Cross-Section Curved Channels," *Combustion and Flame*, V. 159, February, 2012, pp. 859-869.
[17] Paxson, D. E., Kaemming, T. A., "Foundational Performance Analyses of Pressure Gain Combustion Thermodynamic Benefits for Gas Turbines," AIAA 2012-0770, January 2012, also NASA/TM-2012-217443.
[18] Kaemming, T. A., Paxson, D. E., "Determining the Pressure Gain of Pressure Gain Combustion," AIAA-2018-4567, July, 2018.